

Article

Deciphering the Evolution of Adjacent Volcanogenic Massive Sulfide (VMS) Systems Based on Radiogenic and Stable Isotopes, the Case of Ermioni, Argolis Peninsula, Ne Peloponnese, Greece

Stavros Savvas Triantafyllidis ^{1,*}  and Stylianos Fotios Tombros ²

¹ School of Mining and Metallurgical Engineering, National Technical University of Athens, Iroon Polytechniou 9, 157 80 Athens, Greece

² Department of Materials Science, University of Patras, 26504 Rio Patras, Greece

* Correspondence: triantafyllidis@metal.ntua.gr

Abstract: The study follows previous work on Ermioni VMS and addresses in detail the formation and evolution of two adjacent VMS systems, Karakasi and Roro. It is based on a stable and radiogenic isotopic composition of sulfides and gangue from stringer (Karakasi) and massive (Roro) VMS ore. The isotopic geochemistry of Pb and noble gases (Ar-He) of pyrite from both sites indicates the development of a deep and evolved heat and possibly metal source attributed to subduction of radiogenic material (Pindos oceanic crust). The differences in the stable (Fe, S) and radiogenic (Sr, Ar) isotopic compositions between the two sites depict variation in the geologic environment of VMS formation, and in particular the effect of seawater. The higher $\delta^{57}\text{Fe}$ and $\delta^{34}\text{S}$ values of Roro massive pyrite are attributed to direct interaction of hot, ascending metal-bearing hydrothermal fluids with cold seawater. Karakasi stringer ore is characterized by higher $^{87}\text{Sr}/^{86}\text{Sr}$ ratios and radiogenic Ar values (as $^{40}\text{Ar}/^{36}\text{Ar}$), indicating interaction of ore-bearing, hydrothermal fluids with crustal material (hanging-wall turbidites). During the approximate 0.5 Ma period separating the two systems, the hydrothermal system migrated from east to west, and at the same time evolved from free discharge on the seafloor (Roro—easterly), resembling contemporary seafloor style and mound-shaped massive sulfides, to a sediment-confined, subseafloor system (Karakasi—westerly).

Keywords: radiogenic Pb; R/R_A values; ^{57}Fe and ^{34}S isotopes; stringer and massive pyrite; hydrothermal system migration; seafloor and subseafloor VMS formation



Citation: Triantafyllidis, S.S.; Tombros, S.F. Deciphering the Evolution of Adjacent Volcanogenic Massive Sulfide (VMS) Systems Based on Radiogenic and Stable Isotopes, the Case of Ermioni, Argolis Peninsula, Ne Peloponnese, Greece. *Minerals* **2023**, *13*, 474. <https://doi.org/10.3390/min13040474>

Academic Editor: Paolo Nimis

Received: 22 February 2023

Revised: 22 March 2023

Accepted: 24 March 2023

Published: 27 March 2023



Copyright: © 2023 by the authors. Licensee MDPI, Basel, Switzerland. This article is an open access article distributed under the terms and conditions of the Creative Commons Attribution (CC BY) license (<https://creativecommons.org/licenses/by/4.0/>).

1. Introduction

Massive sulfide deposits were among the earliest metallic ore deposits exploited by mankind, namely because of their high grade, texture (massive ore with limited requirements for pre-enrichment), strong contrast with country rocks (especially when surface-exposed outcrops have suffered supergene oxidation), and their relatively simple mining and extraction [1]. The term volcanogenic massive sulfide (VMS) has been in use for nearly 50 years [2] and embraces the temporal and spatial association of sulfide mineralizations with submarine volcanic processes [3]. The generalized structure of VMS deposits includes a “mushroom-shaped”, stratabound, polymetallic, massive sulfide lens (>40 vol. % sulfides) underlain by silica stockworks, known as stringer zones, which function as the feeder zones for the overlying massive ore bodies. Distinctive alteration zones envelope the feeder zones and the massive ore body both vertically and laterally [4]. Most commonly, VMSs are hosted in submarine volcanic and volcanosedimentary successions located at or close to divergent margins [5,6]. According to Barrie et al. [7], they are formed in marine environments after discharge of high-temperature ($T \leq 350\text{ °C}$), metal-enriched hydrothermal fluids onto the seafloor during contact with cold seawater ($\approx 4\text{ °C}$).

Detailed research on VMS deposits has shown that they are characterized by large diversities in ore mineralogy and geochemistry (e.g., base, precious, and strategic metal and metalloid contents), isotopic signature, and host rock lithologies (e.g., [4,8–16]). Subsequently, the most common characteristics shared between the various VMS types are the massive texture of the sulfide ore (regardless of ore mineralogy and geochemistry) and the genetic relation to submarine volcanism.

Although hydrothermal circulation and convection are prerequisites for VMS formation, it is very common for them not to be accompanied by distinctive volcanism at the seafloor, and in many cases the host volcanic and volcanoclastic rocks act only as sources of metals through depletion during hydrothermal convection [17]. Therefore, the geochronological ages calculated by conventional radiogenic isotopes (e.g., zircon U-Th dating, K-Ar on K-bearing silicates) may only provide answers on the age of the hosting volcanic rocks and indirect information on the actual age of ore formation (see [18–20]). This issue has been addressed by recent advances in radiogenic isotope geochronology, and the development of more sophisticated dating methods, including Re-Os, and Pb geochronological dating in sulfides [21,22]. They are considered the most reliable methods for geochronological dating of sulfide ores and have been successfully implemented in VMS deposits (see [19,20,23,24]).

Another major challenge during VMS studies is the identification of the pulses of hydrothermal circulation, as in many cases the mode and the characteristics of VMS formation may change through time, as in the case of the Zn-Pb-Ag deposits of Australia [25], the VMS deposits in the Jinshajiang orogenic belt, southwestern China [26], and the Rudny Altai VMS deposits in Siberia [19]. This is a crucial parameter since the precise definition of the ore-forming system (or systems) not only provides valuable information on other possible deposit types developed in the area under investigation ([3] and references therein) but may also define future exploration strategies.

The objective of the paper is to continue the work of Triantafyllidis et al. [27] regarding the formation of Roro and Karakasi VMS sites from Ermioni area (Figure 1). It is based on previously published data by Triantafyllidis et al. [27] and Tombros et al. [28], and we will show how focused examination of exotic isotopes (both radiogenic and stable) in case-specific phases may provide solid answers on deciphering the origin, development, and evolution of two adjacent VMS systems. The study is relevant for the field of massive sulfide deposits, as the obtained results can be used in the exploration of the marine field to identify new accumulations of useful mineral substances of this type. Moreover, the atypical upper Cretaceous age of the Ermioni VMS relative to neighboring VMS provinces in the Alpine Orogen (e.g., northern Italy [29], and Balkans [30,31]) provides beneficial information on future exploration strategies involving fossilized marine settings of similar age, as in the case of the Kuroko-type VMS deposit of Cerattepe-Artvin in Turkey which is dated to 62 ± 3 Ma ([32,33]). It is worth mentioning that although VMS deposits have been extensively studied, there is very limited work regarding the examination of stable and radiogenic isotopes in specific phases of smaller VMS systems developed within a broader area (see Tornos et al., 2015 [34]). The Ermioni VMS (Figure 1) is a perfect example of such an investigation, as despite its small size and simple mineralogy and geochemistry, there has been a long debate on the actual VMS type this deposit belongs to, and whether it comprises one or more hydrothermal centers. There are a large number of parameters and ore features related to this question, one of them being post-ore deformation and tectonism of the southeast Argolis Peninsula from the Paleocene–Oligocene, that have greatly affected the primary structure of the VMS systems, resulting in dismembered ore bodies scattered within the fine-grained upper Cretaceous–Paleocene turbidites.

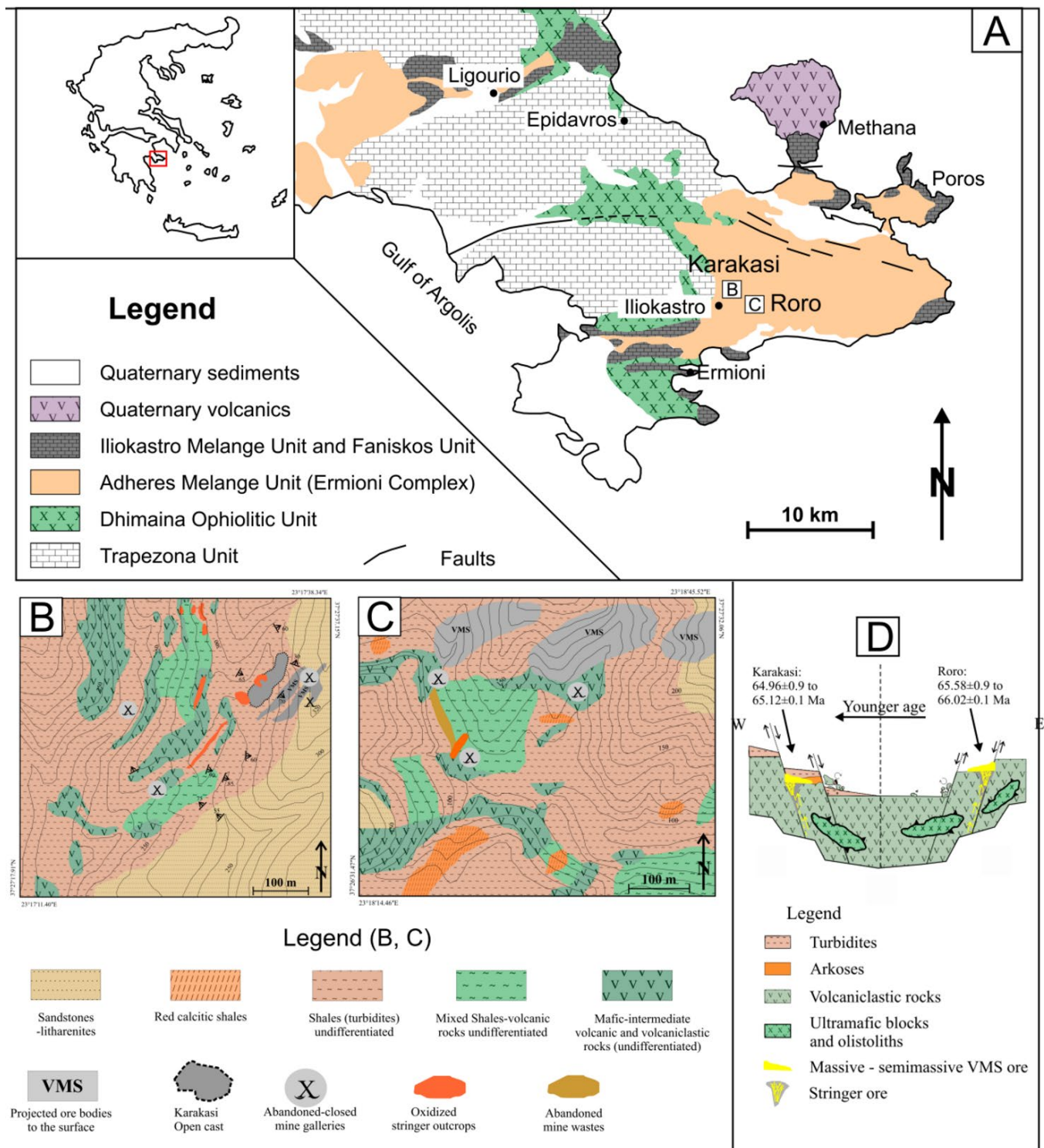


Figure 1. (A) Simplified geologic map of Argolis Peninsula with the locations of the major Ermioni VMS sites (with modifications after [27,35]), (B,C) geology of Karakasi and Roro mining sites (with modifications after [28,36,37]), (D) Simplified geologic map of Ermioni basin in upper Cretaceous during Roro and Karakasi VMS formation (with modifications after [27]).

2. Case Study: The Ermioni VMS

2.1. Argolis Peninsula Regional Geology

The Argolis Peninsula (Figure 1) is an area characterized by complex geology and geodynamic evolution, and several geotectonic and stratigraphic models have been pro-

posed since the late 19th century for the area largely based on conventional geological data [35,36,38–51]. According to the latest views [35], the Argolis Peninsula comprises a metamorphosed Paleozoic basement overlain by five Triassic-to-Paleocene–Eocene nappes [34,52–56] (Figure 1A) including: (a) The lowermost “Trapezona Unit” composed of middle Triassic-to-upper Jurassic neritic carbonates, deep-water limestones, and ophiolite olistostromes, (b) the “Dhimaina Ophiolitic Unit” comprising MORBs covered by Cretaceous limestones and Paleocene–Eocene flysch, (c) the “Adheres Mélange Unit” (also referred as the “Ermioni Complex” by Robertson et al. [50]) composed of ophiolite blocks, volcanic rocks, and late Cretaceous to Paleocene turbidites and carbonates, (d) the “Iliokastron Mélange Unit” consisting of an ophiolite mélange, and (e) the uppermost “Faniskos Unit” composed of upper Cretaceous neritic carbonates.

The difficulty in distinguishing the geotectonic setting and the geodynamic evolution of the southeast Argolis Peninsula is partly linked to the diversity of volcanic rocks that have been identified, including boninites, island arc tholeiites (IAT), and transition (T-MOR) and normal (N-MOR) basalts to name a few [55–61]. In particular, the “Adheres Mélange Unit”, which hosts the Ermioni VMS deposit, comprises ophiolite blocks, ultramafic rocks, calc-alkaline volcanic rocks, boninites, and IAT [48,53]. According to Robertson et al. [50], the boninites and IAT of the Argolis Peninsula depict fore-arc volcanism (subduction initiation) at a Tethys Ocean remnant (Vardar-Axios Ocean) during the late Jurassic–early Cretaceous (Eohellenic phase). During the Cretaceous, the geotectonic setting changed from fore-arc to back-arc, as evident by the calc-alkaline volcanoclastic rocks of the footwall [27].

2.2. Ermioni VMS Deposit Geology and Historical Background

Despite the diverse metallogeny of Greece, only a very small number of VMS mineralizations have been identified, including the Kuroko-type Skra deposit in northern Greece [62–64], and the Molaoi and Ermioni VMS deposits in southern Greece (Peloponnese). The Molaoi VMS is considered a small Kuroko-type mineralization [65], whereas the Ermioni VMS is the only known deposit of this type exploited during the 20th century due to its high pyrite content used for sulfuric acid production for fertilizers. The nearly monomineralic character of the ore with abundant pyrite (>95% modal in the massive ore) and the very low content in As and other volatile and toxic metals made it ideal for such applications [36].

The genetic relation between the massive ore and the host volcanic rocks was supported from very early studies [36,37], and [66–68] have described the Ermioni mineralization as VMS based on early-developed models [2]. Later, Varnavas et al. [69] and Robertson et al. [50] moved one step further and classified it as Cyprus type, mainly based on the ore mineralogy, geochemistry, and the close proximity of the ore to ultramafic lithologies associated with Vardar-Axios Ocean Jurassic ophiolites [54,59]. Nearly 20 years later, Tombros and Seymour [70] and Tombros et al. [71] focused their research on stable isotope geochemistry and the mineral chemistry of sulfides and proposed formation of the Ermioni VMS in a submarine environment analogous to contemporary ocean-ridge black smokers. Recently, Triantafyllidis et al. [27] and Tombros et al. [28] performed a detailed study on the Ermioni VMS, focusing on the most important mine sites, Karakasi and Roro (Figure 1B,C). Their results discarded the previous consensus of the Cyprus-type character of the ore and showed that the Ermioni VMS is actually an atypical “mafic–pelitic” VMS with geochemistry resembling Cyprus-type deposits (Figure 2). The Ermioni VMS was formed due to hydrothermal circulation in a depression of the “Adheres Mélange Unit” (henceforth “Ermioni basin”) in the upper Cretaceous, with abundant pyrite, minor chalcopyrite, and traces of sphalerite ([27,36,37]).

2.3. Karakasi and Roro VMS Geochronology

The Ermioni VMS proved to be very challenging when the age of the ore formation was in question. The mineralogical investigation of the footwall lithologies (mafic–intermediate volcanoclastic rocks) revealed that zircon crystals, K-bearing silicates, or other phases that

could be used for geochronological dating are absent, making the exact dating of the footwall lithologies problematic. Considering these issues and taking into account the previous consensus of the Ermioni VMS, Triantafyllidis et al. [27] focused on radiogenic isotope geochronology of ore-specific cases, and in particular Re-Os dating on pyrite crystals from the massive and stringer ore, and Rb-Sr dating in silicic inclusions in pyrite from both sites (for details, refer to Triantafyllidis et al. [27]). Their Re-Os dating showed that the Ermioni VMS is of upper Cretaceous age. More interestingly, they calculated variations in the ages between the Roro massive (65.58 ± 0.9 to 66.02 ± 0.1 Ma; $2\sigma = \pm 0.98$, MSWD = 0.98, $^{187}\text{Os}_{(i)} = 2.26 \pm 0.03$ and $^{187}\text{Os}/^{188}\text{Os}_{(i)} = 2.18 \pm 0.06$) and the Karakasi stringer ore (64.96 ± 0.9 to 65.12 ± 0.1 Ma; $2\sigma = \pm 1.0$, MSWD = 1.01, $^{187}\text{Os}_{(i)} = 1.83 \pm 0.05$ and $^{187}\text{Os}/^{188}\text{Os}_{(i)} = 1.82 \pm 0.18$), indicating that the Karakasi VMS postdates the Roro VMS by approximately 0.5 Ma. Considering that in a typical VMS structure, the stringer ore predates the overlying massive ore, in the Ermioni area there were at least two different localities where hydrothermal activity was taking place during the upper Cretaceous [27].

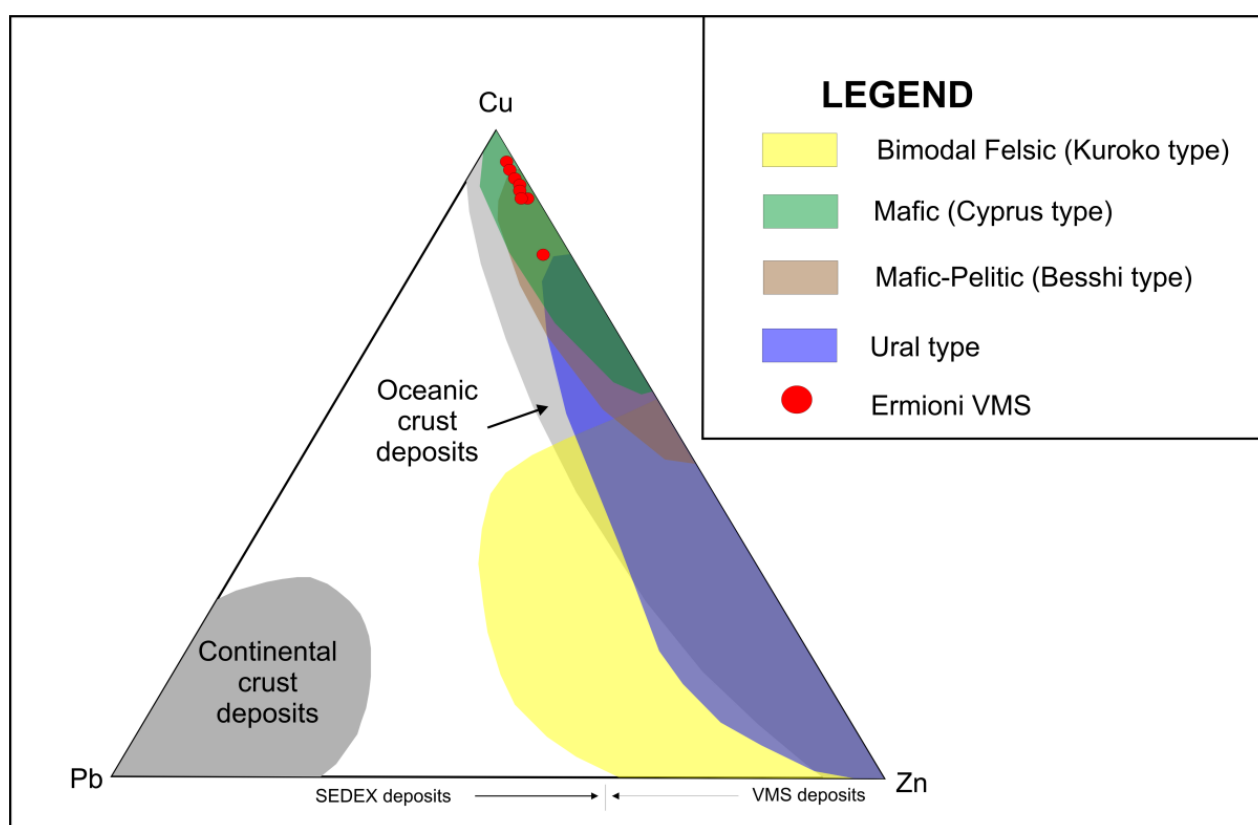


Figure 2. Cu-Pb-Zn ternary diagram of the base-metal composition of various VMS deposit types (data after [4,19]). Red circles depict the massive ore geochemistry of Ermioni mafic–pelitic VMS, plotted in the field of “Cyprus-type” deposits.

3. Analytical Data

The data presented in this study come from the work of Triantafyllidis et al. [27] and come from focused investigation of the stable and radiogenic isotope geochemistry of gangue phases and sulfides from the two most important mine sites, Karakasi and Roro (Figure 1, Tables 1 and 2). Pyrite separates from massive (Roro) and stringer (Karakasi) ore were used for Re-Os, Pb, Rb-Sr (silicic inclusions), He-Ar, Fe, and S isotopic analyses. Details on the analytical techniques, statistical analyses, and software employed can be found in [27].

Table 1. Radiogenic isotope data (Pb, He-Ar, and Rb-Sr) from Ermioni VMS (EK—Karakasi VMS, ER—Roro VMS) (radiogenic isotope data taken from [27]).

Sample	$^{206}\text{Pb}/^{204}\text{Pb}$	$^{207}\text{Pb}/^{204}\text{Pb}$	$^{208}\text{Pb}/^{204}\text{Pb}$	$^4\text{He}^{\text{A}}$	$^3\text{He}^{\text{B}}$	$^{40}\text{Ar}/^{36}\text{Ar}^{\text{C}}$
ER1	18.08	15.6	38.81	4.19	37.05	301.2
ER2	18.06	15.63	38.82	2.5	22.92	315.9
ER3	18.1	15.61	38.82	5.72	49.51	358.1
ER4	18.06	15.61	38.83	3.88	33.05	314.2
ER5	-	-	-	2.49	22.32	331.3
ER12	-	-	-	1.43	12.99	328.8
1 σ	± 0.019	± 0.008	± 0.012	± 1.53	± 12.94	± 19.57
2 σ	± 0.038	± 0.016	± 0.025	± 3.07	± 25.88	± 39.14
St. Error	0.01	0.004	0.006	0.626	5.28	7.99
EK11	18.1	15.63	38.83	1.78	12.98	410.2
EK12	18.1	15.63	38.83	1.55	11.48	453.7
1 σ	-	-	-	± 0.163	± 1.06	± 30.75
2 σ	-	-	-	± 0.326	± 2.12	± 61.51
St. Error	-	-	-	0.115	0.75	21.75
Sample	R/R _A ^D	Rb (ppm)	Sr (ppm)	$^{87}\text{Rb}/^{86}\text{Sr}$	$^{87}\text{Sr}/^{86}\text{Sr}$	
ER1	6.37	0.93	5.98	0.4436	0.7091	
ER2	6.6	1.67	5.36	0.8954	0.7092	
ER3	6.22	0.84	3.78	0.7646	0.7092	
ER4	6.13	1.93	4.12	0.7896	0.7091	
ER5	6.43	1.36	8.04	0.5477	0.7099	
ER12	6.55	1.01	3.56	0.6549	0.7092	
1 σ	± 0.183	± 0.44	± 1.71	± 0.1671	± 0.00074	
2 σ	± 0.367	± 0.88	± 3.41	± 0.3341	± 0.00155	
St. Error	0.074	0.179	0.696	0.0683	0.00032	
EK11	5.24	1.43	10.45	0.5566	0.7103	
EK12	5.34	1.59	9.64	0.5987	0.7109	
1 σ	± 0.071	± 0.11	± 0.57	± 0.0298	± 0.00042	
2 σ	± 0.141	± 0.23	± 1.15	± 0.0595	± 0.00085	
St. Error	0.05	0.08	0.41	0.0211	0.0003	

^A 10^{-7} ; ^B 10^{-13} cm³ STP/g; ^C 10^{-3} ; ^D R_A is the $^3\text{He}/^4\text{He}$ ratio of atmosphere ($^3\text{He}/^4\text{He}$)_{Air} = $1.4 \cdot 10^{-6}$ and ($^4\text{He}/^{36}\text{Ar}$)_{Air} = 0.1655. Typical R/R_A values for MORB are $\sim 8.2 \pm 0.7$ [72], whereas for crust the R/R_A value is ~ 1 [73].

Table 2. Stable isotope data from Ermioni VMS; oxygen and silicon isotopic data were obtained from gangue phases (quartz—Qz, albite—Alb, and calcite—Cal), S and Fe isotopic data were obtained from sulfide separates from massive and stringer ore (EK—Karakasi VMS, ER—Roro VMS, Py—pyrite, Sp—sphalerite) (stable isotope data were taken from [27]).

Sample	Lithotype	Mineral	$\delta^{18}\text{O}_{\text{V-SMOW}}$	$\delta^{30}\text{Si}$
EK1	Volcaniclastic	Qz	+13.11	+1.11
EK2	Volcaniclastic	Alb	+11.42	−0.73
EK3	Volcaniclastic	Qz	+13.84	−0.98
EK4	Volcaniclastic	Qz	+11.22	−0.68
EK5	Volcaniclastic	Qz	+11.95	−1.03
EK6	Volcaniclastic	Qz + cal	+5.06	+0.85
EK7	Stringer ore	Cal	+15.98	−0.47
EK10	Stringer ore	Cal	+17.59	−0.59
1 σ			± 2.42	± 0.82
2 σ			± 4.83	± 1.65
St. Error			0.91	0.29
ER8	Volcaniclastic	Qz	14.12	−0.47
ER10	Volcaniclastic	Qz	+14.43	−0.54
1 σ			± 0.22	± 0.05

Table 2. Cont.

Sample	Lithotype	Mineral	$\delta^{18}\text{O}_{\text{V-SMOW}}$	$\delta^{30}\text{Si}$
2 σ			± 0.44	± 0.1
St. Error			0.16	0.04
Sample	Lithotype	Mineral	$\delta^{34}\text{S}_{\text{VCDT}}$	^{57}Fe
EK1	Volcaniclastic	Py	+0.68	-
EK2	Volcaniclastic	Py	+1.85	-
EK3	Volcaniclastic	Py	+0.54	-
EK4	Volcaniclastic	Py	+4.71	-
EK5	Volcaniclastic	Py	+3.17	-
EK10	Stringer ore	Sp	+1.96	-
EK11	Stringer ore	Py	+5.32	-0.89
EK12	Stringer ore	Py	+4.82	-0.87
1 σ			± 1.87	± 0.01
2 σ			± 3.74	± 0.03
St. Error			0.59	0.01
ER1	Massive ore	Py	+6.21	-0.56
ER2	Massive ore	Py	+5.32	-0.62
ER3	Massive ore	Py	+6.12	-0.67
ER4	Massive ore	Py	+5.93	-0.62
ER5	Massive ore	Py	+5.79	-0.70
ER8	Massive ore	Sp	+3.96	-
ER10	Massive ore	Sp	+2.17	-
ER12	Massive ore	Py	+5.53	-0.77
1 σ			± 1.39	± 0.07
2 σ			± 2.78	± 0.15
St. Error			0.49	0.03

Analytical precision was better than ± 0.1 per mil for $\delta^{18}\text{O}$ and $\delta^{30}\text{Si}$, ± 0.2 per mil for $\delta^{34}\text{S}$, and ± 0.03 per mil for $\delta^{57}\text{Fe}$.

4. Results and Discussion

4.1. Origin of Hydrothermal Fluids

In cases where several hydrothermal venting centers function in different time periods, the radiogenic isotopic signatures of sulfides may be employed in defining the source (or sources) of metals. For Karakasi stringer and Roro massive pyrite, the Pb isotopic values are similar and the $^{206}\text{Pb}/^{204}\text{Pb}$, $^{207}\text{Pb}/^{204}\text{Pb}$, and $^{208}\text{Pb}/^{204}\text{Pb}$ ratios range between 18.06 and 18.10, 15.60 and 15.63, and 38.81 and 38.83, respectively (Table 1), indicating a single and common source of metals (Figure 3A). The Pb radiogenic values for both VMS systems present many similarities to the Pb isotopic signatures of fossilized VMS deposits (e.g., Australian VMS systems [25,74]; Rudny Altai VMS systems [19]; Iberian Pyrite Belt VMS [75]; and modern day black smokers (e.g., Endeavour Segment, Juan de Fuca Ridge [76]; Pito Seamount, Easter Microplate [77]) and are very different to the adjacent and younger in age Cycladic Massif (Aegean Sea) mineralizations related to continental intermediate–felsic magmatism (Figure 3B). The noble gases' isotopic composition of Karakasi and Roro pyrites is typical for VMS sulfides (e.g., Rodriguez Triple Junction, Central Indian Ridge [78]; Southwest Indian Ridge [79]; East Pacific Rise [80]) with R/R_A values ranging between 5.24 and 6.55 (Table 1, Figure 3C), depicting a deep magmatic source affecting the ore-forming hydrothermal fluids [81].

A closer investigation in the Pb and noble gases' isotope geochemistry shows that the Karakasi and Roro pyrites are more radiogenic than enriched mantle (Figure 3A), with $^4\text{He}/^3\text{He}$ values ranging between 108×10^3 and 137×10^3 (Table 1), which in turn are more radiogenic than average MORB ($\approx 90 \times 10^3$ [82,83]), indicating that a possible primitive source with large mantle input is rather improbable [25], especially when considering the geotectonic setting of the Ermioni basin during the Cretaceous. According to Kurz et al. [84], subducting oceanic crust in convergent margins is a possible radiogenic He source. Mougél et al. [80] and Wang et al. [79] state that degassing of oceanic crust takes

place during both formation along ocean ridges and subduction due to generation of high (U+ Th)/³He material. Therefore, the Pb and noble gases' isotopic signature of massive and stringer pyrites could indicate an evolved heat source related to partial melting of subducting radiogenic oceanic crust (Pindos Ocean). This setting is also supported by the trace element geochemistry of the footwall, calc-alkaline volcanoclastic rocks revealing volcanism in a supra-subduction zone setting (SSZ) related to highly evolved magmatism [27]. Both footwall volcanoclastic rocks and the VMS systems under investigation were formed in a similar geotectonic setting including calc-alkaline volcanism in a depression of the Ermioni basin. The textural characteristics of the footwall volcanoclastic rocks (e.g., angular albite fragments, mafic clasts; for details refer to [27,85]) confirm that magmatic activity predated ore formation. Therefore, the Pb and noble gases' isotopic geochemistry of stringer (Karakasi) and massive ore (Roro) pyrite could show depletion of evolved lithologies (footwall volcanoclastic rocks) during hydrothermal convection. Still, we cannot disregard the possibility that magmatic fluids from this deep source (subducting Pindos Ocean) also contributed to the hydrothermal system, as the Pb and noble gases' isotope geochemistry could point to this too.

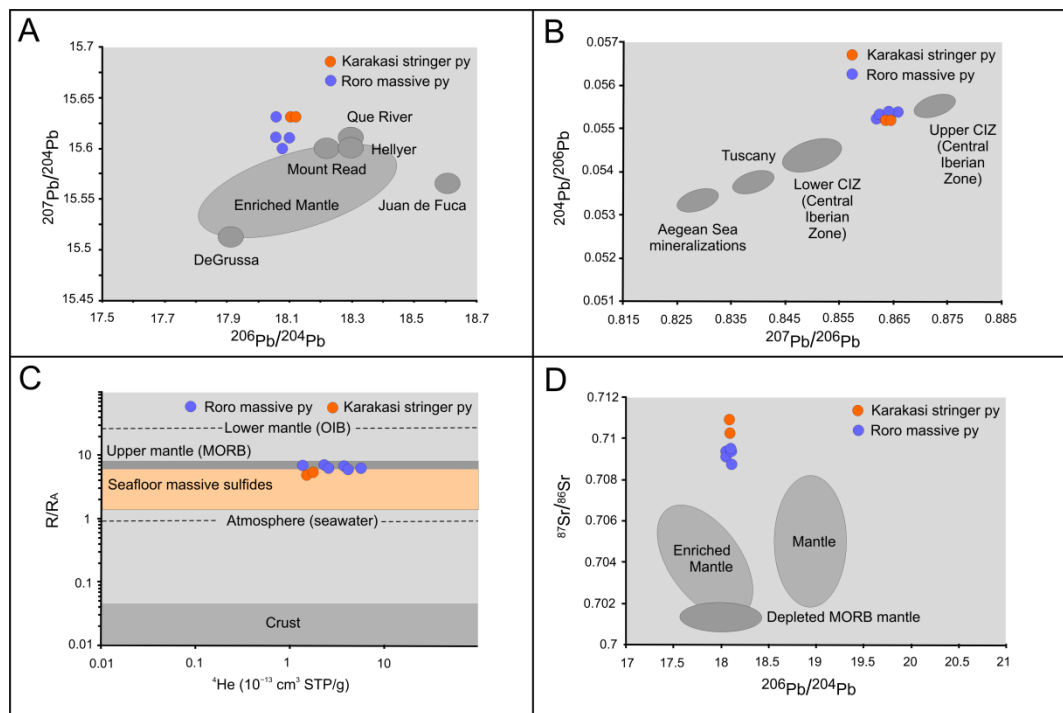


Figure 3. Radiogenic isotope binary diagrams for massive and stringer pyrite from Roro and Karakasi VMS, respectively. (A) $^{206}\text{Pb}/^{204}\text{Pb}$ vs. $^{207}\text{Pb}/^{204}\text{Pb}$ binary diagram of Ermioni VMS pyrite (data from [20,86–89]). (B) $^{207}\text{Pb}/^{206}\text{Pb}$ vs. $^{204}\text{Pb}/^{206}\text{Pb}$ binary diagram of Ermioni VMS pyrite (data from [75,89] and references therein). (C) ^4He vs. R/R_A binary diagram of Ermioni pyrites. The light orange shaded area depicts the range of R/R_A and ^4He values of seafloor massive sulfides (data from [79]). (D) $^{206}\text{Pb}/^{204}\text{Pb}$ vs. $^{87}\text{Sr}/^{86}\text{Sr}$ binary diagram of Ermioni pyrites and silicic inclusions (fields from [87]).

4.2. Geologic Setting of Karakasi and Roro VMS Systems

Despite the common heat source of hydrothermal fluids, there are small, yet distinct differences in the radiogenic (Sr and noble gases) and stable (Fe and S) isotopic compositions between Roro and Karakasi VMS. The $^{87}\text{Sr}/^{86}\text{Sr}$ values of silicic inclusions in Ermioni pyrites (massive and stringer ore) range between 0.7019 and 0.7109, with inclusions from the Karakasi stringer ore having slightly higher $^{87}\text{Sr}/^{86}\text{Sr}$ values relative to Roro massive ore (Table 1, Figure 3D). For both sites, the $\delta^{18}\text{O}$ and $\delta^{30}\text{Si}$ values (Table 2) are higher than

typical MORB, mantle-derived, and differentiation-derived magmas ([90,91] and references therein), proving the incorporation of seawater in the hydrothermal and ore-forming system. Yet, the $\delta^{18}\text{O}$ and $\delta^{30}\text{Si}$ values of hydrothermal quartz from the footwall volcanoclastic rocks at Roro are higher than similar facies at Karakasi VMS (Figure 4A), indicating a higher degree of seawater input in the hydrothermal and ore-forming system. The range of $\delta^{34}\text{S}$ values of sulfides from Karakasi and Roro sites is typical for VMS mineralizations (see [19,32]) (Table 2). For the Karakasi VMS site, the disseminated and stringer pyrite crystals show fluctuations in the S isotopic values, whereas in the Roro massive ore the $\delta^{34}\text{S}$ values for pyrite fall in a narrow range (4.82 to 6.21 per mil) (Figure 4B). Interestingly, sphalerite from both sites (Table 2) is characterized by a lighter $\delta^{34}\text{S}$ isotopic signature (still positive) relative to pyrite. Although the behavior of S isotopes in hydrothermal systems is complex, involving many different factors (e.g., bacterial activity, sulfate reduction during convection), the lower $\delta^{34}\text{S}$ values of late-stage sphalerite could be attributed to a lower seawater contribution, or fractionation of S species during sulfide deposition. According to Tombros et al. [28], the predominance of pyrite in the Karakasi and Roro VMS is attributed to massive input of Fe in the hydrothermal system, a statement supported by the lithologies leached during hydrothermal convection (mafic and ultramafic rocks). The high Fe content of the hydrothermal fluids provokes deposition of pyrite incorporating heavier S isotopes, whereas fractionation during the late stage affects the S isotopic composition of sphalerite (Table 2). The Fe isotope geochemistry of pyrite from Karakasi and Roro VMS also falls in the typical range of values for sulfides from VMS deposits (see [92]). Yet, massive pyrite from Roro VMS shows slightly higher $\delta^{57}\text{Fe}$ values relative to stringer pyrite from Karakasi VMS (-0.56 and -0.77 , and -0.87 and -0.89 , respectively) (Table 2). Comparing the pyrite Fe and S isotopic geochemistry from both sites, the Roro massive pyrite is characterized by slightly higher $\delta^{34}\text{S}$ and $\delta^{57}\text{Fe}$ values relative to Karakasi stringer pyrite (Figure 4B), which is attributed to the interaction of cold seawater with ascending hydrothermal fluids. The degree of interaction differs between the two sites, and is higher in Roro massive and lower in Karakasi stringer ore.

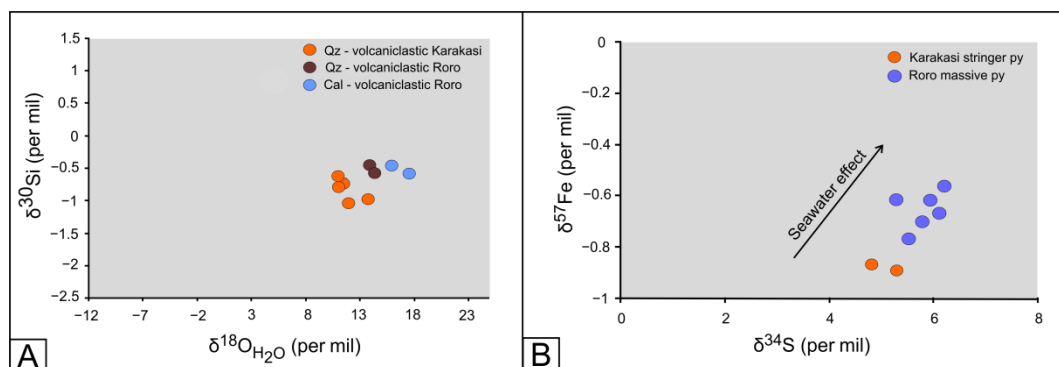


Figure 4. Stable isotope binary diagrams of pyrite and gangue phases from Roro and Karakasi VMS. (A) $\delta^{18}\text{O}$ – $\delta^{30}\text{Si}$ binary diagram of gangue quartz (Qz) and calcite (Cal) from the footwall volcanoclastic rocks from Roro and Karakasi VMS. (B) $\delta^{34}\text{S}$ – $\delta^{57}\text{Fe}$ binary diagram of massive (Roro) and stringer (Karakasi) pyrite from Ermioni VMS (with modifications after [27]).

The early Roro VMS was developed most probably along high-angle normal fault(s) of the eastern part of the Ermioni depression and within the footwall volcanoclastic rocks. The fault(s) acted as feeder zone leading to the formation of the lower stringer ore. Hydrothermal, metal-bearing fluids were fed through these zones and were discharged on the seafloor, causing rapid sulfide deposition after interaction with cold seawater (Figure 5). The aforementioned model of Roro VMS formation is supported by ore texture and stable and radiogenic isotope geochemistry. As stated by Galley et al. [4], the clastic–sandy and fine-grained texture of the Roro massive ore depicts ore deposition on the seafloor, and in particular cementation of loosely held massive ore fragments, later cemented by

quartz and calcite (Figure 5). The R/R_A values of Roro massive pyrite also support direct discharge of hydrothermal fluids on the seafloor without prior interaction with crustal material (e.g., turbidites) (Figure 3C). Moreover, the positive $\delta^{34}\text{S}$ values are also related to direct interaction between hot ascending ore-bearing hydrothermal fluids with cold seawater, thus provoking incorporation of heavier S species in massive pyrite deposited on the seafloor. The higher $\delta^{57}\text{Fe}$ values of massive pyrite from Roro are also attributed to a higher degree of mixing between cold seawater and hot ascending hydrothermal fluids, resulting in increased $\delta^{57}\text{Fe}$ in the late-stage ore-forming system (stage II of [27,28]).

The later (by approx. 0.5 Ma) Karakasi VMS has a different texture relative to Roro VMS. The size of pyrite crystals in the semi-massive to massive ore is greater (>1 mm) (Figure 6) and the hydraulic modeling of [28] showed that hydrothermal convection and ore deposition was taking place within the footwall and hanging-wall lithologies (volcaniclastic rocks, arkoses, and turbidites) [27] (Figure 6A–D). The hydraulic pressure of the system was greater relative to Roro VMS [28], due to the fine-grained character of the hanging-wall turbidites acting as an effective barrier, thus enabling the formation of larger, euhedral pyrite [93,94]. The stable and radiogenic isotope geochemistry of sulfides also supports the views of Tombros et al. [28]. The Sr isotopic composition of silicic inclusions in Karakasi stringer pyrite implies a higher degree of mixing between a low- $^{87}\text{Sr}/^{86}\text{Sr}$ source (e.g., mantle ≈ 0.700) and a high- $^{87}\text{Sr}/^{86}\text{Sr}$ source (oceanic crust/sediments ≈ 0.725), depicting incorporation of crustal material in the ore-forming hydrothermal fluids, attributed to circulation/convection within the unconsolidated fine-grained turbidites of the hangingwall [28] (Figure 6A–D). The noble gases' geochemistry also supports this hypothesis; Karakasi stringer pyrite shows significantly higher Ar values (as $^{40}\text{Ar}/^{36}\text{Ar}$) relative to massive pyrite from Roro VMS (Table 1), indicating more radiogenic Ar incorporation in sulfides (hanging-wall turbidites) [79] (Figure 3C). When compared to Roro massive ore, the lower ^{34}S and ^{57}Fe isotope composition of Karakasi stringer pyrite corresponds to either a lower degree of interaction between penetrating seawater and ascending ore-forming fluids, or formation at higher temperatures [92], which is supported by the ore-forming temperatures (between 330 and 430 °C) calculated by Tombros et al. [28].

During the approximately 0.5 Ma period separating the two VMS systems (Figure 1D), the same, deep-heated hydrothermal system evolved from free discharge on the seafloor (Roro), forming fine-grained massive sulfides, to sediment-confined, subseafloor semi-massive-to-massive pyrite rich masses within unconsolidated turbidites and arkoses. For both locations, seawater was the major component of both hydrothermal systems, yet the seawater effect on the sulfide ore is more prominent in Roro VMS. The latter was developed easterly (based on contemporary coordinates) along normal, high-angle faults, and the metal-bearing fluids were discharged on a seafloor comprising mafic–intermediate volcaniclastic rocks, forming fine-grained massive sulfides (Figure 5). The brittle massive ore suffered limited scale transportation, leading to the development of clastic–sandy texture, in a similar manner to the seafloor style of formation of contemporary mound-shaped massive sulfides. Within the following 0.5 Ma, the VMS-hosting depression in the Ermioni basin was subjected to fine-grained clastic sedimentation (turbidites), that covered the already formed Roro VMS, the volcaniclastic rocks, and the overlying arkoses (based on foraminifera and microfossil species identified in [37,42,54,96]). Contemporaneously to turbidite deposition, the hydrothermal system migrated westwards, finding new pathways through the high-angle normal faults of the western margin of the Ermioni basin and ascended towards the seabed (Figure 6A–D). Convection occurred within the footwall volcaniclastic rocks, arkoses, and the unconsolidated hanging-wall turbidites, leading to the formation of the Karakasi VMS system within the host lithologies. From the Paleocene–Eocene, deformation and tectonism, related to accretion of the Ermioni basin on the Pelagonian continental margin [53], resulted in dismemberment of the Karakasi and Roro VMS systems (Figures 5 and 6). Tectonic separation occurred along discrete ore zones, including the lower stringer zone, and the overlying semi-massive and massive ore, forming small lenses and irregular ore bodies concordant with the hanging-wall turbidites.

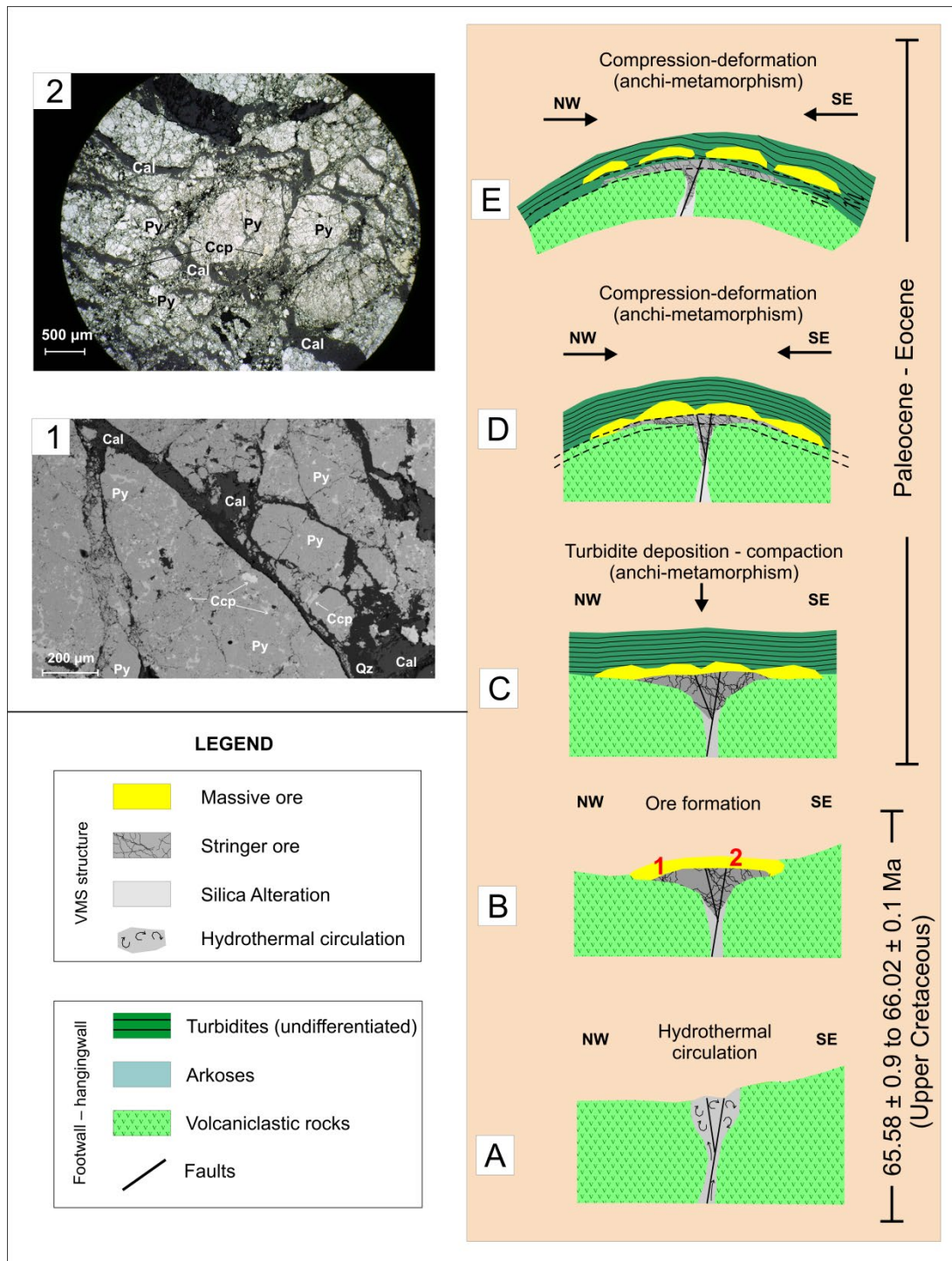


Figure 5. Schematic depiction of the geotectonic evolution of Roro VMS (right side (A–E)). The Roro VMS was formed easterly (relative to Karakasi) on the seafloor prior turbidite deposition resembling the mode of formation of contemporary mound-shaped massive sulfides. (1–2) Photomicrographs of Roro VMS massive ore and their corresponding position in the Roro VMS. (1) SEM-EDS image of massive ore from Roro VMS, with abundant pyrite (Py) and minor chalcopyrite (Ccp). (2) Reflected light optical microscopy image (plain light) of Roro massive ore with typical clastic–sandy texture depicting formation on the seafloor. The angular massive ore fragments with predominant pyrite (Py) and minor chalcopyrite (Ccp) are cemented by later quartz±calcite. (Abbreviations after [95]).

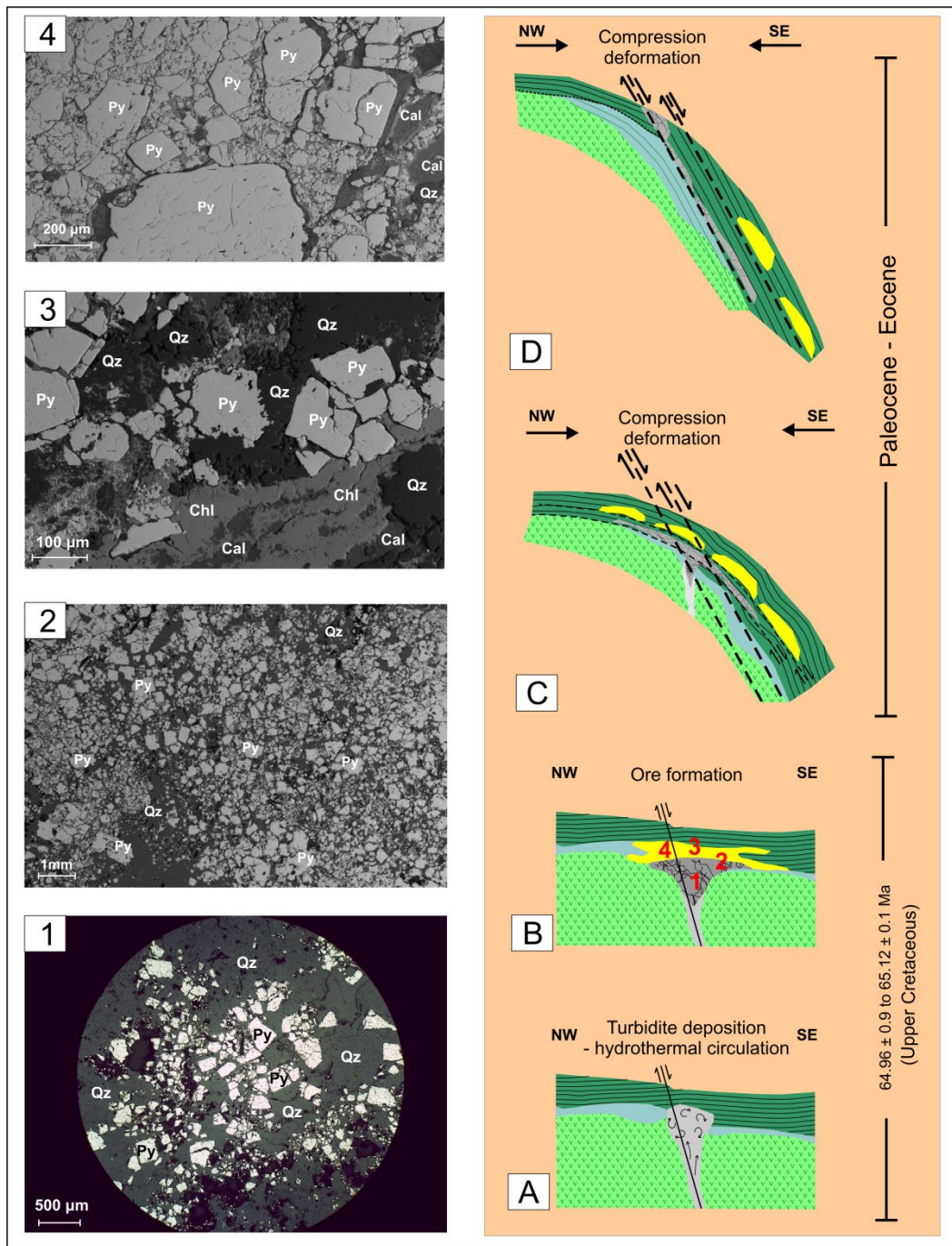


Figure 6. Schematic depiction of the geotectonic evolution of Karakasi VMS (right side (A–D), legend as in Figure 5). The Karakasi VMS was formed later and further west (based on contemporary coordinates) relative to Roro VMS, contemporaneously to arkose and turbidite deposition during upper Cretaceous. (1–4) Photomicrographs of Karakasi VMS ore and corresponding position in the Roro VMS. (1) Disseminated, coarse-grained, euhedral pyrite (Py) and gangue quartz (Qz) from Karakasi stringer ore. (2) Semi-massive pyritic ore (Py) from the transition zone between the lower stringer ore and the upper massive sulfide orebody. Quartz (Qz) is the predominant gangue phase. (3) Semi-massive, coarse-grained, euhedral pyrite (Py) with gangue calcite (Cal), chlorite (Chl), and quartz (Qz). The mineralization is hosted in the hanging-wall turbidites. (4) Massive sulfide ore from Karakasi VMS with abundant pyrite (Py) and gangue calcite (Cal) and quartz (Qz). (Abbreviations after [95]).

The results of this study could be employed in future exploration strategies regarding fossilized upper Cretaceous marine environments in the Alpine Orogen. To this day, the vast majority of VMS mineralizations in the circum-Mediterranean region are considered earlier than the Ermioni VMS (e.g., northern Italy, Balkans, northern Turkey), yet detailed radiogenic studies (Re-Os geochronology) of Kuroko-type VMS in Pontides (northern Turkey, [33]) have shown that the previously accepted ore formation time setting (90–82 Ma) is under question, and upper Cretaceous ages are now accepted. This proves the importance of detailed investigation of upper Cretaceous marine environments, with beneficial results for the metallogenic potential of the eastern Mediterranean.

5. Conclusions

The Ermioni VMS is a perfect example of the mode of evolution of VMS-related hydrothermal systems in geologically active areas, and how focused examination of stable and radiogenic isotopes in specific cases may be employed in providing answers regarding genesis and evolution of hydrothermal systems, their mixing with various sources, the geologic environment of hydrothermal circulation/convection, and VMS formation. Examination of the Karakasi and Roro VMS systems in the Ermioni area revealed the following:

1. The Pb and noble gases' (Ar-He) isotopic geochemistry of massive (Roro) and stringer (Karakasi) pyrite indicates a deep and evolved heat source, which probably also acted as a source of metals, attributed to subduction and partial melting of a radiogenic He source (depleted Pindos Oceanic crust).
2. Despite the unknown age of footwall volcanoclastic rocks, the radiogenic isotope composition of massive and stringer pyrite indicates a similar geotectonic setting for both footwall volcanoclastic rocks and the VMS systems.
3. This study shows how stable (Fe, S) and radiogenic (Pb, Sr, Ar) isotopic examination focused on specific phases may be used in the identification of both the source of metals and the setting of VMS ore formation. In the case of Ermioni VMS, the stable and radiogenic isotope compositions of VMS pyrite from Karakasi (stringer ore) and Roro (massive ore) point to differences in the geologic environment of VMS formations. Roro massive pyrite shows higher $\delta^{57}\text{Fe}$ and $\delta^{34}\text{S}$ values relative to Karakasi stringer pyrite, attributed to direct interaction of ascending metal-bearing hydrothermal fluids with cold seawater. Karakasi stringer pyrite shows higher $^{87}\text{Sr}/^{86}\text{Sr}$ ratios and radiogenic Ar values (as $^{40}\text{Ar}/^{36}\text{Ar}$) depicting the interaction of hydrothermal fluids with crustal material (hanging-wall turbidites).
4. During the approximately 0.5 Ma period separating the two systems, the same hydrothermal and ore-forming system evolved from free discharge on the seafloor (Roro—easterly) to a sediment-confined, subseafloor system (Karakasi—westerly). The Roro massive ore resembles a seafloor style of formation of contemporary mound-shaped massive sulfides, whereas the later Karakasi VMS hosted in the footwall and hanging-wall lithologies points to hydrothermal circulation within the Ermioni basin floor lithologies.
5. The results of this study can be used during exploration of fossilized upper Cretaceous marine environments of the Alpine Orogen, with corresponding benefits in the metallogenic potential of the eastern Mediterranean.

Author Contributions: Conceptualization, S.S.T.; methodology, S.S.T. and S.F.T.; software, S.F.T.; validation, S.S.T. and S.F.T.; formal analysis, S.S.T. and S.F.T.; investigation, S.S.T. and S.F.T.; resources, S.S.T. and S.F.T.; data curation, S.S.T. and S.F.T.; writing—original draft preparation, S.S.T.; writing—review and editing, S.S.T.; visualization, S.S.T. and S.F.T.; supervision, S.S.T. and S.F.T.; project administration, S.S.T. All authors have read and agreed to the published version of the manuscript.

Funding: This research received no external funding.

Data Availability Statement: Not applicable.

Acknowledgments: The authors would like to thank the anonymous reviewers for their insightful and valuable comments during the development of the manuscript.

Conflicts of Interest: The authors declare no conflict of interest.

References

1. Shanks, W.C.P., III. Historical Evolution of Descriptive and Genetic Knowledge and Concepts. In *Volcanogenic Massive Sulfide Occurrence Model*; Shanks, W.C.P., III, Thurston, R., Eds.; Scientific Investigations Report, 2010–5070–C; USGS: Reston, VA, USA, 2012; pp. 23–32.
2. Hutchinson, R.W. Volcanogenic sulfide deposits and their metallogenic significance. *Econ. Geol.* **1973**, *68*, 1223–1246. [[CrossRef](#)]
3. Koski, R.A.; Mosier, D.L. Deposit type and associated commodities. In *Volcanogenic Massive Sulfide Occurrence Model*; Shanks, W.C.P., III, Thurston, R., Eds.; Scientific Investigations Report, 2010–5070–C; USGS: Reston, VA, USA, 2012; pp. 15–21.
4. Galley, A.G.; Hannington, M.D.; Jonasson, I.R. Volcanogenic massive sulphide deposits. In *Mineral Deposits of Canada: A Synthesis of Major Deposit-Types, District Metallogeny, the Evolution of Geological Provinces, and Exploration Methods*; Goodfellow, W.D., Ed.; Geological Association of Canada, Mineral Deposits Division, Special Publication: St. John's, NL, Canada, 2007; pp. 141–161.
5. Lydon, J.W. Volcanogenic massive sulphide deposits Part 1: A descriptive model. *Geosc. Can.* **1984**, *11*, 195–202.
6. Sawkins, F.J. *Metal Deposits in Relation to Plate Tectonics*, 2nd ed.; Springer: New York, NY, USA, 1990.
7. Barrie, C.T.; Cathles, L.M.; Erendi, A.; Schwaiger, H.; Murray, C. Heat and Fluid Flow in Volcanic-associated Massive Sulfide-Forming Hydrothermal Systems. In *Volcanic-Associated Massive Sulfide Deposits: Processes and Examples in Modern and Ancient Settings*; Barrie, C.T., Hannington, M.D., Eds.; Society of Economic Geologists: Littleton, CO, USA, 1999; Volume 8. [[CrossRef](#)]
8. Leistel, J.M.; Marcoux, E.; Thiéblemont, D.; Quesada, C.; Sánchez, A.; Almodóvar, G.R.; Pascual, E.; Sáez, R. The volcanic-hosted massive sulphide deposits of the Iberian Pyrite Belt, Review and preface to the Thematic Issue. *Miner. Depos.* **1998**, *33*, 2–30. [[CrossRef](#)]
9. Barrie, C.T.; Hannington, M.D. (Eds.) Introduction: Classification of VMS deposits based on host rock composition. In *Volcanic-Associated Massive Sulfide Deposits: Processes and Examples in Modern and Ancient Settings*; Society of Economic Geologists: Littleton, CO, USA, 1999; Volume 8. [[CrossRef](#)]
10. Franklin, J.M.; Hannington, M.D. Volcanogenic massive sulfides through time. In Proceedings of the Annual Meeting, Abstracts with Programs, Denver, CO, USA, 27–30 October 2002; Volume 34, p. 283.
11. Gibson, H.L.; Allen, R.L.; Riverin, G.; Lane, T.E. The VMS model: Advances and application to exploration targeting. In Proceedings of the Exploration 07: 5th Decennial International Conference on Mineral Exploration, Toronto, ON, Canada, 9–12 September 2007; pp. 717–730.
12. Pirajno, F.; Seltmann, R.; Yang, Y. A review of mineral systems and associated tectonic settings of northern Xinjiang, NW China. *Geosc. Front.* **2011**, *2*, 157–185. [[CrossRef](#)]
13. Piercey, S. The setting, style and role of magmatism in the formation of volcanogenic massive sulfide deposits. *Min. Depos.* **2011**, *46*, 449–471. [[CrossRef](#)]
14. Ross, P.-S.; Mercier-Langevin, P. The volcanic setting of VMS and SMS deposits: A review. *Geosc. Can.* **2014**, *41*, 365–377. [[CrossRef](#)]
15. Martin-Izard, A.; Arias, D.; Arias, M.; Gumiel, P.; Sanderson, D.J.; Castañón, C.; Sanchez, J. Ore deposit types and tectonic evolution of the Iberian Pyrite Belt: From transtensional basins and magmatism to transpression and inversion tectonics. *Ore Geol. Rev.* **2016**, *79*, 254–267. [[CrossRef](#)]
16. Hollis, S.P.; Yeats, C.J.; Wyche, S.; Barnes, S.J.; Ivanic, T.J.; Belford, S.M.; Davidson, G.J.; Roache, A.J.; Wingate, M.T.D. A review of volcanic-hosted massive sulfide (VHMS) mineralization in the Archaean Yilgarn Craton, Western Australia: Tectonic, stratigraphic and geochemical associations. *Precamb. Res.* **2019**, *260*, 113–135. [[CrossRef](#)]
17. Schulz, K.J. Regional Environment. In *Volcanogenic Massive Sulfide Occurrence Model*; Shanks, W.C.P., III, Thurston, R., Eds.; Scientific Investigations Report, 2010–5070–C; USGS: Reston, VA, USA, 2012; pp. 37–60.
18. Mousivand, F.; Rastad, E.; Meffre, S.; Peter, J.M.; Mohajjel, M.; Zaw, K.; Emami, M.H. Age and tectonic setting of the Bavanat Cu–Zn–Ag Besshi-type volcanogenic massive sulfide deposit, southern Iran. *Miner. Depos.* **2012**, *47*, 911–931. [[CrossRef](#)]
19. Lobanov, K.V.; Yakubchuk, A.; Creaser, R.A. Besshi-type VMS deposits of the Rudny Altai (Central Asia). *Econ. Geol.* **2014**, *109*, 1403–1430. [[CrossRef](#)]
20. Hawke, M.L.; Meffre, S.; Stein, H.; Hilliard, P.; Large, R. Geochronology of the DeGrussa volcanic-hosted massive sulphide deposit and associated mineralisation of the Yerrida, Bryah and Padbury Basins, Western Australia. *Precamb. Res.* **2015**, *267*, 250–284. [[CrossRef](#)]
21. Stein, H.J.; Morgan, J.W.; Scherstén, A. Re–Os dating of low-level highly-radiogenic (LLHR) sulfides: The Harnäs gold deposit, southwest Sweden records continental scale tectonic events. *Econ. Geol.* **2000**, *95*, 1657–1671. [[CrossRef](#)]
22. Yang, J.-H.; Zhou, X.-H. Rb–Sr, Sm–Nd and Pb isotope systematics of pyrite: Implications for the age and genesis of lode gold deposits. *Geology* **2001**, *29*, 711–714. [[CrossRef](#)]
23. Nozaki, T.; Kato, Y.; Suzuki, K. Re–Os geochronology of the Iimori Besshi-type massive sulfide deposit in the Sanbagawa metamorphic belt, Japan. *Geochim. Cosmochim. Acta* **2010**, *74*, 4322–4331. [[CrossRef](#)]

24. Pirajno, F.; Chen, Y.; Li, N.; Li, C.; Zhou, L. Besshi-type mineral systems in the Palaeoproterozoic Bryah Rift-Basin, Capricorn Orogen, Western Australia: Implications for tectonic setting and geodynamic evolution. *Geosci. Front.* **2016**, *7*, 345–357. [[CrossRef](#)]
25. Huston, D.L.; Stevens, B.; Southgate, P.N.; Muhling, P.; Wyborn, L. Australian Zn-Pb-Ag Ore-Forming Systems: A Review and Analysis. *Econ. Geol.* **2006**, *101*, 1117–1157. [[CrossRef](#)]
26. Zengqian, H.; Liqian, W.; Zaw, K.; Xuanxue, M.; Mingjie, W.; Dingmou, L.; Guitang, P. Post-collisional crustal extension setting and VHMS mineralization in the Jinshajiang orogenic belt, southwestern China. *Ore Geol. Rev.* **2003**, *22*, 177–199. [[CrossRef](#)]
27. Triantafyllidis, S.; Tombros, S.F.; Zhai, D.; Kokkalas, S. The Upper Cretaceous Ermioni VMS Deposit, Argolis Peninsula, Peloponnese, Greece: Type, genesis, and geotectonic setting. *Ore Geol. Rev.* **2021**, *138*, 104403. [[CrossRef](#)]
28. Tombros, S.F.; Triantafyllidis, S.; Kokkalas, S.; Fitros, M.; Zhai, D.; Papavasiliou, J.; Spiliopoulou, A.; Kappis, K.; Skliros, V.; Perraki, M. Hydraulic-Thermodynamic Modeling of the upper Cretaceous “Mafic-Pelitic” Ermioni VMS deposit, Greece. *Ore Geol. Rev.* **2022**, *148*, 105039. [[CrossRef](#)]
29. Kiss, G.B.; Molnár, K.; Benkó, Z.; Skoda, P.; Kapui, Z.; Garuti, G.; Zaccarini, F.; Palcsu, L.; Czuppon, G. Tracing the Source of Hydrothermal Fluid in Ophiolite-Related Volcanogenic Massive Sulfide Deposits: A Case Study from the Italian Northern Apennines. *Minerals* **2023**, *13*, 8. [[CrossRef](#)]
30. Bogdanov, K.; Tsonev, D.; Kuzmanov, K. Mineralogy of gold in the Elshitsa massive sulphide deposit, Sredna Gora zone, Bulgaria. *Mineral. Depos.* **1997**, *32*, 219–229. [[CrossRef](#)]
31. Economou-Eliopoulos, M.; Eliopoulos, D.G.; Chrysosoulis, S. A comparison of high Au massive sulfide ores hosted in ophiolite complexes of the Balkan Peninsula with modern analogues: Genetic significance. *Ore Geol. Rev.* **2008**, *33*, 81–100. [[CrossRef](#)]
32. Revan, M.K.; Maslennikov, V.V.; Genç, Y.; Delibaş, O.; Maslennikova, S.P.; Sadykov, S.A. Sulfur isotope study of vent chimneys from Upper Cretaceous volcanogenic massive sulfide deposits of the eastern Pontide metallogenic belt, NE Turkey. *Turk. J. Earth Sci.* **2016**, *25*, 227–241. [[CrossRef](#)]
33. Ucurum, A.; Demir, C.S.; Otlu, N.; Erturk, M.; Ekici, T.; Kirk, J.; Ruiz, J.; Mathur, R.; Arehart, G.B. Re-Os Age and Stable Isotope (O-H-S-Cu) Geochemistry of North Eastern Turkey’s Kuroko-Type Volcanogenic Massive Sulfide Deposits: An Example from Cerattepe-Artvin. *Minerals* **2021**, *11*, 226. [[CrossRef](#)]
34. Tornos, F.; Peter, J.M.; Allen, R.; Conde, C. Controls on the sitting and style of volcanogenic massive sulphide deposits. *Ore Geol. Rev.* **2015**, *68*, 142–163. [[CrossRef](#)]
35. Bortolotti, V.; Carras, N.; Chiari, M.; Fazzuoli, M.; Marcucci, M.; Photiades, A.; Principi, G. New geological observations and biostratigraphic data on the Argolis Peninsula: Paleographic and geodynamic implications. *Ophioliti* **2002**, *27*, 43–46.
36. Aronis, G. *Research on the Iron-Pyrite Deposits in the Hermioni Mining District, Geological and Geophysical Surveys*; Subsurface Research Department, Ministry of Coordination: Athens, Greece, 1951; pp. 153–188, (In Greek with English Abstract).
37. Mousoulos, L. Les gisements pyriteux du district minier d’Hermione. Étude sur leur géologie et minéralogie. Le problème de leur genèse. *Ann. Géol. Pays Hellén.* **1958**, *9*, 119–164.
38. Philippson, A. *Der Peloponnes: Versuch Einer Landeskunde auf Geologischer Grundlage*; R. Frielander: Berlin, Germany, 1892.
39. Renz, C. Trias und jura in der Argolis. *Zeitschr. Deutsch. Geol. Ges.* **1906**, *58*, 379–395.
40. Ktenas, C. Formations primaires semimetamorphiques du Peloponnese Central. *Comptes Rendus Geosci. Société Géologique Fr.* **1917**, *24*, 61–63.
41. Marinos, G. Das auftreten granitischer gesteine in Argolis (Ermioni) and das Alter der Schiefersandsteinformation. *Bull. Geol. Soc. Gr.* **1955**, *2*, 121–123.
42. Aranitis, S. Beiträge zur kenntis der geologie des gebietes von Hermionis (Griecheland). *Bull. Geol. Soc. Greece* **1963**, *4*, 97–105.
43. Mercier, J. Étude géologique des zones internes des Hellénides en Macédoine central (Grèce). Contribution à l’ etude du metamorphisme et de l’évolution magmatique des zones internes des Hellénides. Thésés, Paris. *Ann. Géol. Pays Hellén.* **1968**, *20*, 1–792.
44. Aubouin, J.; Bonneau, M.; Celet, P.; Charvet, J.; Clement, B.; DeGardin, J.M.; Dercourt, J.; Ferrière, J.; Fleury, J.J.; Guernet, C. Contribution à la géologie des Hellénides: Le Gavrovo, le Pinde et la zone ophiolitique subpélagonienne. *Ann. Soc. Géol. Nord.* **1970**, *90*, 277–306.
45. Celet, P.; Ferrière, J. Les Hellénides internes: Le Pélagonien. *Eclogae Geol. Helv.* **1978**, *71*, 467–495.
46. Jacobshagen, V.; Dürr, S.; Kockel, F.; Kopp, K.O.; Kowalczyk, S. Structure and geodynamic evolution of the Aegean region. In *Alps, Apennines, Hellenides*; Closs, H., Roeder, D., Schmidt, K., Eds.; Schweizerbart: Stuttgart, Germany, 1978; pp. 537–564.
47. Varnavas, S.P.; Panagos, A.G. Mesozoic metalliferous sediments from the ophiolites of Ermioni, Greece: Analogue to recent mid-ocean ridge ferromanganese deposits. *Chem. Geol.* **1984**, *42*, 227–242. [[CrossRef](#)]
48. Baumgartner, P.O. Jurassic sedimentary evolution and nappe emplacement in the Argolis Peninsula (Peloponnesus, Greece). *Mém. Soc. Helv. Sci. Nat.* **1985**, *99*, 1–111.
49. Photiades, A. Contribution à l’ étude géologique et métallogénique des unités ophiolitiques de l’ Argolide septentrionale (Grèce). Ph.D. Thesis, Université de Besancon, Besancon, France, 1986.
50. Robertson, A.H.F.; Varnavas, S.P.; Panagos, A.G. Ocean ridge origin and tectonic setting of Mesozoic sulphide and oxide deposits of the Argolis peninsula of the Peloponnesus, Greece. *Sedim. Geol.* **1987**, *53*, 1–32. [[CrossRef](#)]
51. Clift, P.D.; Robertson, A.H.F. Evidence of a late Mesozoic Ocean basin and subduction/accretion in southern Greek Neo-Tethys. *Geology* **1989**, *17*, 559–563. [[CrossRef](#)]
52. Robertson, A.H.F.; Clift, P.D.; Degnan, P.J.; Jones, G. Palaeogeographic and palaeotectonic evolution of the eastern Mediterranean Neotethys. *Palaeogeogr. Palaeoclim. Palaeoecol.* **1991**, *87*, 289–343. [[CrossRef](#)]

53. Clift, P.D.; Dixon, J.E. Jurassic ridge collapse, subduction initiation and ophiolite obduction in the southern Greek Tethys. *Ecol. Geol. Helv.* **1998**, *91*, 128–138. [[CrossRef](#)]
54. Bortolotti, V.; Carras, N.; Chiari, M.; Fazzuoli, M.; Marcucci, M.; Photiades, A.; Principi, G. The Argolis peninsula in the paleogeographic and geodynamic frame of the Hellenides. *Ofioliti* **2003**, *28*, 79–94.
55. Saccani, E.; Padoa, E.; Photiades, A. Tectono-magmatic significance of Triassic MORBs from the Argolis Peninsula (Greece): Implication for the origin of the Pindos Ocean. *Ofioliti* **2002**, *27*, 73–74.
56. Saccani, E.; Photiades, A.; Padoa, E. Geochemistry, petrogenesis and tectono-magmatic significance of volcanic and subvolcanic rocks from the Koziakas mélangé (Western Thessaly, Greece). *Ofioliti* **2003**, *28*, 43–67.
57. Photiades, A. The diversity of Jurassic volcanism in the inner parts of the Hellenides: The northern Argolis ophiolitic units (Peloponnese, Greece). *Bull. Geol. Soc. Greece* **1989**, *23*, 515–530.
58. Dostal, J.; Toscani, L.; Photiades, A.; Capedri, S. Geochemistry and petrogenesis of Tethyan ophiolites from northern Argolis (Peloponnesus, Greece). *Eur. J. Min.* **1991**, *3*, 105–121. [[CrossRef](#)]
59. Photiades, A.D.; Economou, G.S. Clinopyroxene and spinel composition of ophiolitic volcanic rocks (Southern Argolis Peninsula, Greece): Implications for the geodynamic evolution. *Bull. Geol. Soc. Greece* **1992**, *28*, 69–83.
60. Clift, P.D. Accretion tectonics of the Neotethyan Ermioni Complex, Peloponnesos, Greece. *J. Geol. Soc.* **1996**, *153*, 745–757. [[CrossRef](#)]
61. Bortolotti, V.; Chiari, M.; Marcucci, M.; Marroni, M.; Pandolfi, L.; Principi, G.; Saccani, E. Comparison among the Albanian and Greek ophiolites: In search of constraints for the evolution of the Mesozoic Tethys Ocean. *Ofioliti* **2004**, *29*, 19–35.
62. Tsamantouridis, P.; Polychronakis, I. *Reconnaissance Report on the Mineralogy of the Skra Area, Kilikis Prefecture*; Report in Greek, Athens, No 2488; Institute of Geology and Mineral Exploration of Greece: Thessaloniki, Greece, 1977; unpublished.
63. Tsamantouridis, P.; Polychronakis, I. *Annual Report (1979) on the Results of Exploratory Works at Public Grant F9 and the Skra Area (Kilikis Prefecture)*; Report in Greek, Athens, No 3150; Institute of Geology and Mineral Exploration of Greece: Thessaloniki, Greece, 1980; 16p, unpublished.
64. Tsamantouridis, P. *Study of the Sulphide Mineralization of Eastern Paikon Area (Kilikis District)*; Institute of Geology and Mineral Exploration of Greece, Mineral Deposit Research (in Greek): Thessaloniki, Greece, 1980; Volume 13, 39p.
65. Skarpelis, N. Massive Sulfide Metallogeny and Petrology of the External Metamorphic Zone of the Hellenides. Ph.D. Thesis, National Kapodistrian University of Athens, Zografou, Greece, 1982. (In Greek with English Abstract).
66. Skounakis, S.; Sovatzoglou-Skounakis, E. The Co and Ni traces distribution within the deposits of Cu-bearing pyrite of Ermioni, Argolida. *Ann. Géol. Pays Hellén.* **1975**, *13*, 54–60.
67. Skounakis, S.; Sovatzoglou-Skounakis, E. The Co-content of pyrite and chalcopyrite as geothermometer for the Cu-bearing pyrite ore deposits of Hermione's (Argolis) and Perivoli's (Pindos) areas, Greece. *Ann. Géol. Pays Hellén.* **1982**, *31*, 89–94.
68. Sideris, C.; Skounakis, S. Metallogeny in the basic rocks of a paleosubduction area-The case of Ermioni Cu-bearing pyrite mines (East Peloponnesos, Greece). *Chem. Erde* **1987**, *47*, 93–96.
69. Varnavas, S.P.; Panagos, A.G.; Philippakis, G. On the metallogenesis of the Hermioni area, Greece. Mesozoic mid-ocean ridge deposits. *Geol. Carpath.* **1985**, *36*, 219–233.
70. Tombros, S.F.; Seymour, K. Hermione, evolution of a Te-bearing epithermal mineralization, Argolis, Hellas. *Bull. Geol. Soc. Greece* **2007**, *40*, 996–1008. [[CrossRef](#)]
71. Tombros, S.F.; Seymour, K.; Spry, P.G.; William-Jones, A.E. Karakasi mines, Hermione, evolution of a Cyprus-type Cu-Zn deposit, Argolis, Greece. In Proceedings of the Digging Deeper, 9th Biennial SGA Meeting, Dublin, Scotland, 20–23 August 2007.
72. Hilton, D.R.; Hammerschmidt, K.; Loock, G.; Friedrichsen, H. Helium and argon isotope systematics of the central Lau Basin and Valu Fa Ridge: Evidence of crust/mantle interactions in a back-arc basin. *Geochim. Cosmochim. Acta* **1993**, *57*, 2819–2841. [[CrossRef](#)]
73. Yuce, G.; Taskiran, L. Isotope and chemical compositions of thermal fluids at Tekman geothermal area (Eastern Turkey). *Geochem. J.* **2013**, *47*, 423–435. [[CrossRef](#)]
74. Morey, A.A.; Bierlein, F.P.; Cherry, D.P.; Turner, G. Genesis of greenstone-hosted Cu–Au mineralisation at Hill 800, Mt Useful Slate Belt, eastern Victoria. *Austr. J. Earth Sci.* **2002**, *49*, 787–799. [[CrossRef](#)]
75. Albarede, F.; Blichert-Toft, J.; Gentelli, L.; Milot, J.; Vaxevanopoulos, M.; Klein, S.; Westner, K.; Birch, T.; Davis, G.; de Gallatay, F. A miner's perspective on Pb isotope provenances in the Western and Central Mediterranean. *J. Arch. Sci.* **2020**, *12*, 105194. [[CrossRef](#)]
76. Yao, H.-Q.; Zhou, H.-Y.; Peng, X.-T.; Bao, S.-X.; Wu, Z.-J.; Li, J.-T.; Sun, Z.-L.; Chen, Z.-Q.; Chen, G.-Q. Metal sources of black smoker chimneys, Endeavour Segment, Juan de Fuca Ridge: Pb isotope constraints. *Appl. Geochem.* **2009**, *24*, 1971–1977. [[CrossRef](#)]
77. Verati, C.; Lancelot, J.; Hékinian, R. Pb isotope study of black-smokers and basalts from Pito Seamount site (Easter microplate). *Chem. Geol.* **1999**, *155*, 45–63. [[CrossRef](#)]
78. Gamo, T.; Chiba, H.; Yamanaka, T.; Okudaira, T.; Hashimoto, J.; Tsuchida, S.; Ishibashi, J.; Kataoka, S.; Tsunogai, U.; Okamura, K. Chemical characteristics of newly discovered black smoker fluids and associated hydrothermal plumes at the Rodriguez Triple Junction, Central Indian Ridge. *EarthPlanet. Sci. Lett.* **2001**, *193*, 371–379. [[CrossRef](#)]
79. Wang, Y.; Han, X.; Qiu, Z. Source and nature of ore-forming fluids of the Edmond hydrothermal field, Central Indian Ridge: Evidence from He–Ar isotope composition and fluid inclusion study. *Acta Oceanol. Sin.* **2018**, *36*, 101–108. [[CrossRef](#)]
80. Mougél, B.; Moreira, M.; Agranier, A. A “high $^4\text{He}/^3\text{He}$ ” mantle material detected under the East Pacific Rise ($15^\circ 4' \text{N}$). *Geophys. Res. Lett.* **2015**, *42*, 1375–1383. [[CrossRef](#)]

81. Hopp, J.; Trieloff, M.; Buikin, A.I.; Korochantseva, E.V.; Schwarz, W.H.; Althaus, T.; Altherr, R. Heterogeneous mantle argon isotope composition in the subcontinental lithospheric mantle beneath the Red Sea region. *Chem. Geol.* **2007**, *240*, 36–53. [[CrossRef](#)]
82. Allègre, C.J.; Moreira, M.; Staudacher, T. $^4\text{He}/^3\text{He}$ dispersion and mantle convection. *Geophys. Res. Lett.* **1995**, *22*, 2325–2328. [[CrossRef](#)]
83. Graham, D.W. Noble gases in geochemistry and cosmochemistry. In *Reviews in Mineralogy and Geochemistry*; Porcelli, D., Wieler, R., Ballentine, C., Eds.; Mineralogical Society of America: Washington, DC, USA, 2002; pp. 247–318.
84. Kurz, M.D.; Jenkins, W.J.; Hart, S.R.; Clague, D. Helium isotopic variations in volcanic rocks from Loihi seamount and the Island of Hawaii. *Earth Planet. Sci. Lett.* **1983**, *66*, 388–406. [[CrossRef](#)]
85. Triantafyllidis, S. Trace element geochemistry, mineralogy and texture of the Ermioni VMS mineralization host volcanics, and new insights on the geotectonic setting of volcanism, Argolis, Greece. *Bull. Geol. Soc. Greece* **2019**, *7*, 321–322.
86. Sangster, D.F.; Outridge, P.M.; Davis, W.J. Stable lead isotope characteristics of lead ore deposits of environmental significance. *Environ. Rev.* **2000**, *8*, 115–147. [[CrossRef](#)]
87. Hoffmann, A.W. Sampling Mantle Heterogeneity through Oceanic Basalts: Isotopes and Trace Elements. In *Treatise in Geochemistry*; Turekian, K.K., Holland, H.D., Eds.; Elsevier: Amsterdam, The Netherlands, 2003. [[CrossRef](#)]
88. Ridley, W.I. Geochemical characteristics. In *Volcanogenic Massive Sulfide Occurrence Model*; Shanks, W.C.P., III, Thurston, R., Eds.; Scientific Investigations Report, 2010–5070–C; USGS: Reston, VA, USA, 2012; pp. 207–225.
89. Müller, R.; Brey, G.P.; Seitz, H.-M.; Klein, S. Lead isotope analyses on Late Republican sling bullets. *Archaeol. Anthropol. Sci.* **2015**, *7*, 473–485. [[CrossRef](#)]
90. Bindeman, I. Oxygen Isotopes in Mantle and Crustal Magmas as Revealed by Single Crystal Analysis. *Rev. Min. Geoch.* **2008**, *69*, 445–478. [[CrossRef](#)]
91. Kleine, B.I.; Stefánsson, A.; Halldórsson, S.A.; Whitehouse, M.J.; Jónasson, K. Silicon and oxygen isotopes unravel quartz formation processes in the Icelandic crust. *Geochem. Lett.* **2018**, *7*, 5–11. [[CrossRef](#)]
92. Syverson, D.D.; Luhmann, A.J.; Tan, C.; Borrok, D.M.; Ding, K.; Seyfried, W.E., Jr. Fe isotope fractionation between chalcopyrite and dissolved Fe during hydrothermal recrystallization: An experimental study at 350 °C and 500 bars. *Geochim. Cosmochim. Acta* **2017**, *200*, 87–109. [[CrossRef](#)]
93. Raiswell, R. Pyrite texture, isotopic composition and the availability of iron. *Am. J. Sci.* **1982**, *282*, 1244–1263. [[CrossRef](#)]
94. Passier, H.F.; Middelburg, J.J.; De Lange, G.J.; Böttcher, M.E. Pyrite contents, microtextures, and sulfur isotopes in relation to formation of the youngest eastern Mediterranean sapropel. *Geology* **1997**, *25*, 519–522. [[CrossRef](#)]
95. Whitney, D.L.; Evans, B.W. Abbreviations for names of rock-forming minerals. *Amer. Miner.* **2010**, *95*, 185–187. [[CrossRef](#)]
96. Bachmann, G.H.; Risch, H. Die geologischeentwicklung der Argolis-Halbinsel (Peloponnes, Griechenland). *Geol. Jb.* **1979**, *B32*, 3–177.

Disclaimer/Publisher’s Note: The statements, opinions and data contained in all publications are solely those of the individual author(s) and contributor(s) and not of MDPI and/or the editor(s). MDPI and/or the editor(s) disclaim responsibility for any injury to people or property resulting from any ideas, methods, instructions or products referred to in the content.